Stem cell therapy for cardiovascular disease : answering basic questions regarding cell behavior

Bogt, K.E.A. van der

CHAPTER 2

Multimodal evaluation of *in vivo* magnetic resonance imaging of myocardial restoration by mouse embryonic stem cells

Stephen L. Hendry III*, Koen E.A. van der Bogt*, Ahmad Y. Sheikh, Takayasu Arai, Scott J. Dylla, Micha Drukker, Michael V. McConnell, Ingo Kutschka, Grant Hoyt, Feng Cao, Irving L. Weissman, Andrew J. Connolly, Marc P. Pelletier, Joseph C. Wu, Robert C. Robbins and Phillip C. Yang

Journal of Thoracic and Cardiovascular Surgery

2008 Oct;136(4):1028-1037.

*Both authors contributed equally to this study

ABSTRACT

Objective: Mouse embryonic stem cells (mESC) have demonstrated the potential to restore the infarcted myocardium following an acute myocardial infarction (AMI). Although the underlying mechanism remains controversial, MRI has provided reliable *in vivo* assessment of functional recovery following cell transplantation. Multi-modality comparison of the restorative effects of mESC and mouse embryonic fibroblasts (mEF) was performed to validate MRI data and provide mechanistic insight.

Methods: SCID beige mice (n=55) underwent coronary artery ligation followed by injection of $2.5x10^5$ mESC, $2.5x10^5$ mEF, or normal saline (NS). *In vivo* MRI of myocardial restoration by mESC was evaluated by: 1) *in vivo* pressure volume (PV) loops, 2) *in vivo* bioluminescence imaging (BLI), and 3) *ex vivo* TaqMan PCR (TM-PCR) and immunohistology.

Results: *In vivo* MRI indicated significant improvement of LVEF at 1 week in the mESC group. This finding was validated with: (1) PV loop analysis demonstrating significantly improved systolic and diastolic functions, (2) BLI and TM-PCR showing superior post-transplant survival of mESC, (3) immunohistology identifying cardiac phenotype within the engrafted mESC, and (4) TM-PCR measuring increased expression of angiogenic and anti-apoptotic genes, and decreased expression of anti-fibrotic genes.

Conclusion: This study validates *in vivo* MRI as an effective modality to evaluate the restorative potential of mESC.

INTRODUCTION

Cellular therapy is rapidly emerging as a potential therapeutic option following an acute myocardial infarction (AMI).[1] Although studies have shown that transplantation of stem cells derived from different lineages have provided significant functional recovery in the setting of AMI, the exact mechanisms of cell-mediated restoration have not been established.[2] There are several theories regarding the possible mechanisms underlying myocardial restoration following cell therapy: 1) augmentation of the infarct region's elasticity preserving regional systolic and diastolic functions; 2) contractility of engrafted cells improving systolic function; 3) angiogenesis enhancing regional myocardial perfusion; and 4) paracrine effects modulating the progression of cardiac remodeling.[3-6]

In vivo MRI has demonstrated improved cardiac function following transplantation of stem cells in both pre-clinical and clinical investigations.[1, 7-11] These findings have led to questions regarding the validity of such data, however, and more importantly, the potential mechanisms underlying myocardial restoration. This investigation addresses these issues by validating *in vivo* MRI evaluation of myocardial restoration through a systematic comparison of the restorative potential of "non-specific" mouse embryonic fibroblasts (mEF) to the more biologically active, self-renewing, pluripotent mouse embryonic stem cells (mESC) in a murine model of AMI. This is the first study to validate *in vivo* MRI at a functional level, and to conduct a multimodality evaluation of physiologic, cellular, and molecular mechanisms of mESC-mediated myocardial restoration.

METHODS

Cell culture. Undifferentiated D3-derived mESC (ATCC, Manassas, VA) were cultured in DMEM (Invitrogen, Carlsbad, CA) with 15% fetal calf serum (FCS, Hyclone, Logan, UT), 100 mg/mL penicillin-streptomycin, 1mM sodium pyruvate, 2mM L-glutamine, NEAA, 0.1mM b mercaptoethanol (Invitrogen, Carlsbad, CA) and 106 u/mL leukemia inhibitory factor (Chemicon International, Temecula, CA). Fresh mouse embryonic fibroblasts (mEF) were prepared from 13-day embryos, whose carcasses were minced and passed 10 times through a 21-gauge needle. Cells were seeded in 10 cm culture dishes and were propagated for two passages in DMEM with 10% FCS and 100 mg/mL penicillin-streptomycin solution. Both mESC and mEF were transfected with a lentiviral vector carrying a cytomegalovirus promoter driving both a firefly luciferase (fluc) reporter gene and green fluorescent protein (GFP). Cells underwent FACS sorting for GFP and single clone selection; the clone was adapted to feeder-free conditions. Prior to injection, the cells were trypsinized (0.25% trypsin/0.02% EDTA) washed with DMEM containing 10% serum. Following centrifugation, the cells were washed with PBS, centrifuged and resuspended in PBS for injection one hour after trypsinization.

Experimental animals. Animal care and interventions were provided in accordance with the Laboratory Animal Welfare Act, the *Guide for the Care and Use of Laboratory Animals* (National Institutes of Health, publication 78-23, revised 1978). Immunotolerant SCID-beige female mice (8-12 weeks, Charles River, Wilmington, MA) were anesthetized in an isoflorane inhalational chamber and endotracheally intubated with a 20 gauge angiocath (Ethicon Endo-Surgery, Inc. Cincinnati, OH). Ventilation was maintained with a Harvard rodent ventilator. Myocardial infarction was created by ligation of the mid-left anterior descending (LAD) artery through a left thoracotomy. The mice were randomized into three groups: 1) LAD ligation with normal saline (NS) injection (n=10), 2) LAD ligation with mESC injection (n=25), or 3) LAD ligation with mEF injection (n=20). The infarct region was injected with 25mL using a Hamilton syringe containing 250,000 mESC, mEF, or NS. Cell suspensions contained rhodamine beads (6×10^5) to ensure injection accuracy. Following chest tube placement, the chest was closed in 2 layers with 5-0 vicryl.

***In vivo* MRI.** One week after transplantation, cardiac MRI was obtained using a Unity Inova console (Varian, Inc., Palo Alto, CA) controlling a 4.7T, 15cm horizontal bore magnet (Oxford Instruments, Ltd., Oxford, UK) with GE Techron Gradients (12G/cm) and a volume coil with a diameter of 3.5cm (Varian, Inc., Palo Alto, CA). The ECG gating was optimized using 2 subcutaneous precordial leads with respiratory motion and body temperature monitors (SA Instruments, Inc., Stony Brook, NY). LV function was evaluated using ECG-triggered cine sequence (TE 2.8-ms, TR 160-ms, FA 60°, FOV 3.0cm2, matrix 128×128, slice gap 0-mm, slice thickness 1.0-mm, 8 NEX, and 12 cardiac phases). The imaging plane was localized using double-oblique acquisition. The data were analyzed using MR Vision software (Winchester, MA). LV ejection fraction (LVEF), end-diastolic (LVED), and end-systolic (LVES) volumes were calculated by tracing the endocardial borders in end-systole and -diastole.

Pressure-volume (PV) loop analysis. One week after transplantation, ventricular performance was assessed by PV loop analysis using a 1.4 F conductance catheter (Millar Instruments, Houston, TX) prior to euthanasia. The closed chest technique was utilized which consisted of a midline neck incision to access the left external jugular vein with PE10 tubing (Intramedic-Becton Dickinson). The right carotid was cannulated with the Millar catheter and advanced through the aortic valve into the LV. The PV relations were measured at baseline and during inferior vena cava occlusion. The measurements of segmental conductance were recorded which allowed extrapolation of the left ventricular volume. When coupled with pressure, the generation of ventricular PV relationships allowed precise hemodynamic characterization of ventricular systolic and diastolic function and loading conditions.[12] These data were analyzed using PVAN 3.4 Software (Millar Instruments, Inc.) and Chart/Scope Software (AD Instruments, Inc.).

***In vitro* firefly luciferase (fluc) assay.** On the day of operation, parallel sets of cells from the same plates as the injected cells were trypsinized, resuspended in PBS and divided into a 6-well plate in different concentrations. After administration of D-luciferin (Xenogen, California, USA, 4.5ug/mL), peak signal expressed as photons per second per centimeter square per steridian (p/s/cm^2/sr) was measured using a charged coupled device (CCD) camera (Xenogen, California, USA).

***In vivo* optical bioluminescence imaging (BLI).** Optical BLI was performed using 8 x 5 minute acquisition scans on a CCD camera (IVIS 50, Xenogen, California, USA). Recipient mice were anesthetized and placed in the imaging chamber. After acquisition of a baseline image, mice were intraperitoneally injected with D-luciferin (Xenogen, USA, 400 mg/kg body weight). Peak signal (p/s/cm^2/sr) from a fixed region of interest (ROI) was evaluated using the Living Image 2.50 software (Xenogen, USA).

***Ex vivo* TaqMan PCR (TM-PCR) for cell survival and expression of genes of interest.** Since the transplanted cells were derived from male mice and were transplanted into female recipients, the surviving mESC in the explanted hearts could be quantified using TM- PCR to track the SRY locus found on the Y chromosome. Whole explanted hearts were minced and homogenized in DNAzol (Invitrogen, Carlsbad, CA). RNA was extracted from the mice myocardium after treatment with TRIzol reagent (Invitrogen, Carlsbad, CA). Taqman PCR was performed using SuperScript II RT-PCR kit (Invitrogen, Carlsbad, CA). To assess the expression of several genes of interest, relative quantitation of mouse primers was performed for: matrix metalloproteinase (MMP)-1β, -2, -9, -14, tumor necrosis factor (TNF)-α, vascular endothelial growth factor (VEGF)-A, procollagen-2α1, transforming growth factor (TGF)-β, angiotensin converting enzyme (ACE), insulin-like growth factor (IGF) 1, Flk-1, and NFkβ-1 (Applied Biosystems, Foster City, CA). The fluorogenic probes contained a 5'-FAM report dye and 3'-BHQ1 quencher dye. TaqMan 18S Ribosomal RNA (Applied Biosystems, Foster City, CA) was used as control gene. RT-PCR reactions were conducted in iCylcer IQ Real-Time Detection Systems (Bio-Rad, Hercules, CA).

Histological analysis. Hearts were flushed with NS and subsequently placed in 2% paraformaldehyde for 2 hours at room temperature followed by 12-24 hours in 30% sucrose at 4°C. The tissue was embedded in Optical Cutting Temperature (OCT) Compound (Tissue-Tek. Sakura Finetek USA Inc., Torrance, CA) and snap frozen on dry ice. Five-micron sections were cut in both the proximal and apical regions of the infarct zone. Slides were stained for H&E, GFP (anti-green fluorescent protein, rabbit IgG fraction, anti-GFP Alexa Fluor 488 conjugate, 1:200, Molecular Probes, Inc.), Troponin I (H-170 rabbit polyclonal IgG for cardiac muscle, 1:100, Santa

Cruz Biotech, Santa Cruz, CA), and Connexin 43 (rabbit polyclonal, 1:100, Sigma). Stained tissue was examined by Leica DMRB fluorescent microscope and a Zeiss LSM 510 two-photon confocal laser scanning microscope. Cell engraftment was confirmed by identification of GFP expression under fluorescent microscopy. Colocalization of troponin, alpha sarcomeric actin, and connexin 43 with GFP was visualized with streptavidin-conjugated to Alexa Fluor Red 555 (Invitrogen Molecular Probes, Carlsbad, CA).

Statistical analysis. Descriptive statistics included mean and standard error. Comparison between groups was performed using students' t-test for independent and normally distributed data variables using SPSS 11.0. For comparison between multiple groups, ANOVA with Bonferroni correction was utilized. Significance was assumed when $p<0.05$.

RESULTS

Quantitation of left ventricular ejection fraction (LVEF) by *in vivo* MRI. As seen in **figure 1a and b**, MRI indicated that AMI led to significant reduction in LVEF at 1 week in all groups compared to sham operated, normal hearts [60.9±1.4% (n=5)] ($p<0.01$), illustrating the effectiveness of this murine AMI model. A significant improvement of LVEF in the mESC-treated [40.2 ±2.0% (n=23)] group was seen versus mEF- [29.4 ± 1.5% (n=17)] and NS-treated [26.4 ± 1.8% (n=6)] ($p<0.05$) groups. No significant improvement was observed in the mEF- versus NS-treated group. Measurements of LV end-diastolic and –systolic volumes are included in **Table 1**.

Measurement of maximal elastance (EMax) and end systolic elastance (Ees) by pressure-volume (PV) loop analysis. As seen in **figure 1c**, PV loop analysis demonstrated significantly compromised Emax (mmHg/mL) in the mEF- [9.95 ± 1.4 (n=4)] and NS-treated [5.8 ± 1.2 (n=4)] groups compared to normal hearts [22.6 ± 2.5 (n=5)] ($p<0.05$) at 1 week. However, a preserved Emax (mmHg/mL) was noticeable in the mESC-treated group [18.4 ± 3.5 (n=4)], which was significantly higher than the mEF- and NS-treated groups ($p<0.05$). No significant improvement was observed in Emax in the mEF- versus the NS-treated group. The Ees data paralleled these findings with a significant decrease in the NS-treated [4.1 ± 0.7 (n=4)] group versus normal hearts [12.5 ± 1.2 (n=5)] ($p<0.05$) and a significant preservation of Ees in the mESC-treated [8.8 ± 1.5 (n=4)] versus the mEF- and NS-treated groups ($p<0.05$). No significant improvement was observed in Ees in the mEF- versus NS-treated group. As shown in **figure 1d**, the left ventricular volumes measured by PV-loop in the mEF and NS groups demonstrate negative remodeling, while mESC treated hearts showed the least dilatation. The improved systolic and diastolic functions measured by the PV loops provide physiologic confirmation of *in vivo* MRI data, as left ventricular volumes measured by MRI and PV loop correlate (**figure 1e**). For further results of invasive hemodynamic measurements, please refer to **Table 1**.

	Normal	mESC	mEF	NS
MRI				
LVEF (%)	60.9 ± 1.4	40.2 ±2.0	29.4 ± 1.5	26.4 ± 1.8
LVED volume (mL)	4.23 ± 0.5	4.53 ± 0.6	5.74 ± 0.6	8.32 ± 0.7
LVES volume (mL)	1.63 ± 0.2	2.67 ± 0.2	4.09 ± 0.3	6.14 ± 0.5
PV-Loop				
Heart rate (bpm)	277.25 ± 10.60	302.75 ± 26.93	319.25 ± 16.45	260.00 ± 22.51
End-systolic Volume (uL)	26.72 ± 0.49	21.65 ± 4.82	40.56 ± 8.67	45.82 ± 8.89
End-diastolic Volume (uL)	29.29 ± 0.47	24.00 ± 5.56	43.15 ± 9.21	49.40 ± 9.67
End-systolic Pressure (mmHg)	83.86 ± 9.17 †	85.92 ± 5.91 †	71.40 ± 6.55	49.84 ± 5.35
End-diastolic Pressure (mmHg)	5.15 ± 1.21	19.14 ± 7.01	6.50 ± 0.54	8.21 ± 1.64
Arterial Elastance (Ea) (mmHg/uL)	29.34 ± 9.50	37.50 ± 11.56	22.04 ± 3.88	10.62 ± 3.35
dPdt max (mmHg/sec)	4100.50 ± 412.10	3867.50 ± 751.61	3108.75 ± 293.20	2157.00 ± 358.83
dPdt min (mmHg/sec)	-2993.25 ± 138.66 †	-2779.75 ± 144.06 †	-2397.75 ± 107.80	-1578.50 ± 304.29
Tau_w (msec)	15.01 ± 1.32	21.38 ± 4.32	15.13 ± 1.16	12.75 ± 3.89
Maximal Power (mWatts)	0.79 ± 0.10	0.78 ± 0.07	1.15 ± 0.45	0.84 ± 0.27
Preload adjusted maximal power (mWatts/µL^2)	9.21 ± 1.19	18.88 ± 6.13 †	5.87 ± 0.76	3.69 ± 1.25

Table 1. Steady-state hemodynamic measurements by MRI and PV-loop. † indicates $p<0.05$ vs. NS (†), no symbols indicate p=NS (ANOVA).

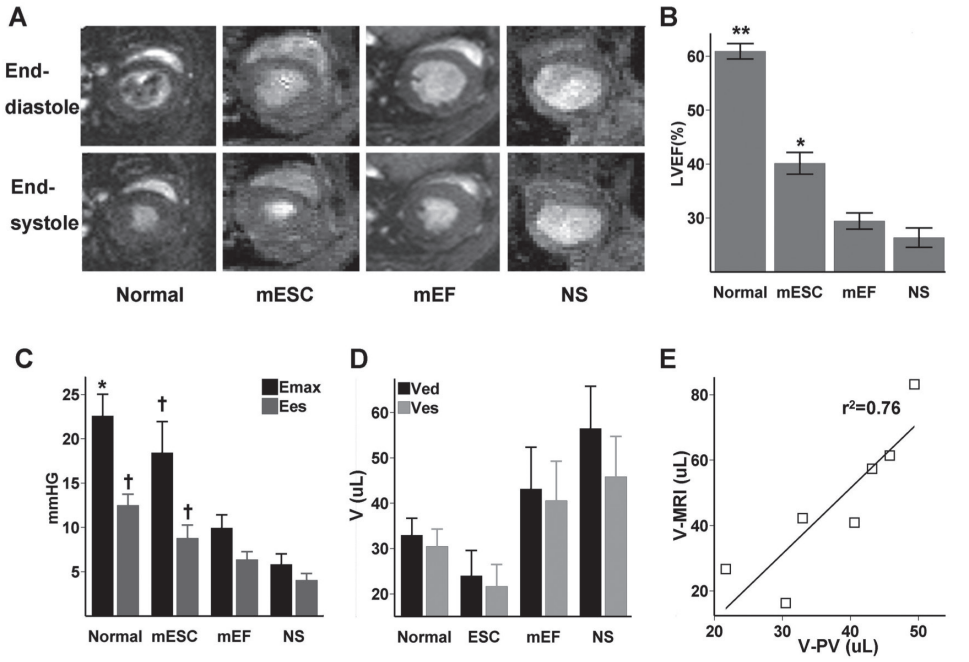

Figure 1. Functional outcomes after mESC and mEF transplantation. (a) Representative MR images of each group (normal, mESC, mEF, and NS) shown in end-diastole and end-systole at one week after LAD ligation and cell transplantation. The mESC-treated group demonstrated increased LVEF with visual confirmation from the MR images. (b) One week after LAD ligation and cell transplantation, MRI indicated significant improvement in the left ventricular ejection fraction (LVEF) in the mESC versus mEF and NS groups. ** Indicate $p<0.01$ vs. all groups, * represents $p<0.05$ vs. MEF and NS (ANOVA). (c) One week after LAD ligation and cell transplantation, PV loop analysis demonstrated compromised Emax (mmHg/μL) in the mEF and NS groups compared to normal hearts. A preserved Emax (mmHg/μL) was noticeable in the mESC group, which was significantly higher than the NS group. No significant improvement was observed in Emax in the mEF group versus the NS group. The Ees data show significant decrease in the NS group versus normal hearts and a significant preservation of Ees in the mESC group versus the NS group. No significant improvement was observed in the mEF group versus NS. * Indicates $p<0.05$ vs. mEF and NS, † indicates $p<0.05$ vs. NS ($n>4$/ group, ANOVA). (d) PV loop measurements of left ventricular volumes in end-systole (Ves) and end-diastole (Ved) show a decreased ventricular dilatation in the mESC group (p=NS). (e) Scatter plot of average left ventricular volumes in each group measured by PV loop (V-PV) and MRI (V-MRI), with r^2=0.76.

Determination of transplanted cell survival by *in vivo* BLI and *ex vivo* TaqMan PCR. Stable mESC and mEF transfection with GFP and firefly luciferase (fluc) generated mESC-GFP$^+$-fluc$^+$ and mEF-GFP$^+$-fluc$^+$ cell lines. The cells were selected and tested for fluc signal by bioluminescence imaging (BLI). Expression of fluc signal correlated robustly with cell number (r^2=0.99 and r^2=0.95, respectively, **figure 2a-c**). Thus, BLI was validated as a tool to monitor cell viability quantitatively as the signal intensity reflected the number of viable cells *in vitro*. Following transplantation of the transfected cells, BLI signal from the mESC-treated group decreased until post operative day (POD) 2. At POD 8 and 14, there was a significant ($p<0.01$) increase in signal due to the rapid division of the undifferentiated mESC (**figure 3a-b**); probably commencing teratoma formation as already shown in our earlier work.[13] However, in the mEF-treated group, signal increased until POD 2 but decreased thereafter, suggesting cell death (**figure 3a-b**). *Ex vivo* TaqMan PCR (TM-PCR) results indicated significantly lower cycle numbers over time in the mESC-treated group compared to the increasing cycle numbers in the mEF-treated group (**figure 3c**), which is representative of higher number of viable male donor cells in the mESC group.[14] Thus, *ex vivo* TM-PCR correlated well with the BLI results (**figure 3d**). This finding supports *in vivo* MRI data in which cell survival, a major biological property, is significantly enhanced in order for the transplanted mESC to remain biologically active to restore the injured myocardium.

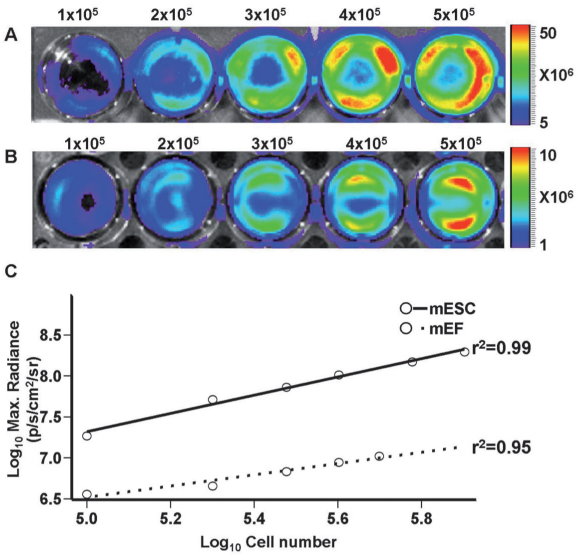

Figure 2. *In Vitro* Firefly Luciferase (fluc) signal correlates with cell number. (a, b) Bioluminescence (BLI) image showing increasing fluc signal with increasing cell number in mouse embryonic stem cells (mESC, a) and embryonic fibroblasts (mEF, b). Bars represent maximum radiance (p/s/cm^2/sr). (c) Correlation plot showing robust correlation of fluc signal and cell number for mESC and mEF (r^2=0.99 and r^2=0.95, respectively).

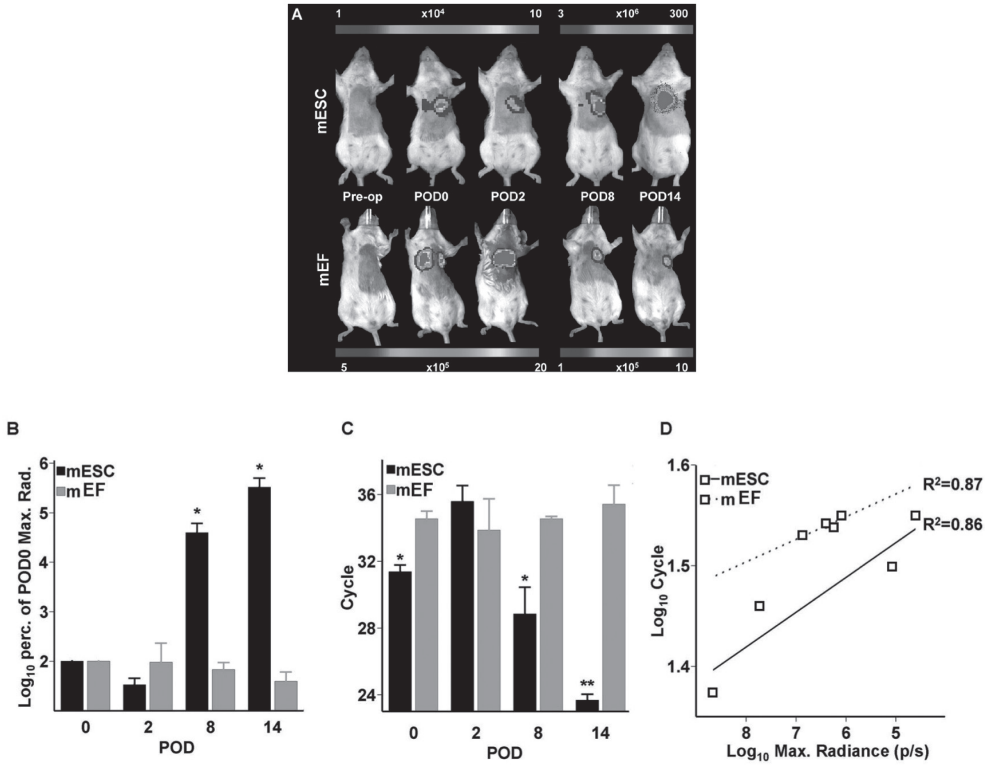

Figure 3. Transplanted Cell Survival by *in vivo* Bioluminescence and ex vivo TaqMan PCR. (a) Representative BLI images of mESC survival, tracked longitudinally at post-operative day (POD) 0, 2, 8, and 14. The survival decreases from POD 0 to POD 2 after which there is a notable increase at POD 8 and 14 due to rapid division. Color bars represent maximum radiance (p/s/cm^2/sr). (b) Normalized plot indicating significant ($p<0.01$) mESC proliferation starting on POD 2 and gradual cell death in the mEF group starting on POD 2 ($n>4$/group). Y-axis shows the $\log_{10}$ percentage of the average BLI signal on POD 0. * Indicates $p<0.01$ vs. mESC on POD 0, 2, and all mEF time points (ANOVA). (c) Ex vivo TaqMan PCR for SRY gene representing the male mESC survival at POD 0, 2, 8, and 14 which demonstrates a similar trend as seen in the *in vivo* BLI ($n>4$/group). * Indicates $p<0.05$ vs. mEF, ** indicate $p<0.01$ vs. mEF (ANOVA). (d) Correlation plot showing correlation ($r^2=0.86$ and $r^2=0.87$ for mESC and mEF, respectively) between *in vivo* BLI and ex vivo TaqMan PCR.

Gene expression profiling by TM-PCR for matrix metalloproteinase (MMP)-1β, -2, -9, -14, tumor necrosis factor (TNF)-a, vascular endothelial growth factor (VEGF)-A, procollagen-2a1, insulin-like growth factor (IGF) 1, transforming growth factor (TGF) -b, angiotensin converting enzyme (ACE), Flk-1, and NFkβ-1. Relative quantitation of mRNA expression of 12 genes (4 mice/group) using RT-PCR demonstrated significant increase of TNF-a in the mESC-treated group when compared to mEF- and NS-treated groups (501% vs. 77% and 219%, respec-

tively, p<0.01). Significant up-regulation of VEGF-A was also observed in mESC-treated group compared to the mEF and NS-treated groups (104% vs. 13% and 42%, respectively, p<0.01). On the other hand, mESC-treated mice demonstrated a trend towards down-regulation of MMP-1β and procollagen-2α1 expression when compared to NS-treated groups (p>0.05). The mRNA expressions of the remainder of genes; IGF1, NFkβ-1, MMP-2, -9, -14, TGFb, ACE, and Flk-1 did not demonstrate significant difference among mESC- mEF- and NS-treated groups. The gene expression profiles of TNF-α, which may have had an enhanced anti-apoptotic effects, and VEGF-A, consistent with proangiogenic effects, were demonstrated in the mESC-treated group (**figure 4**).

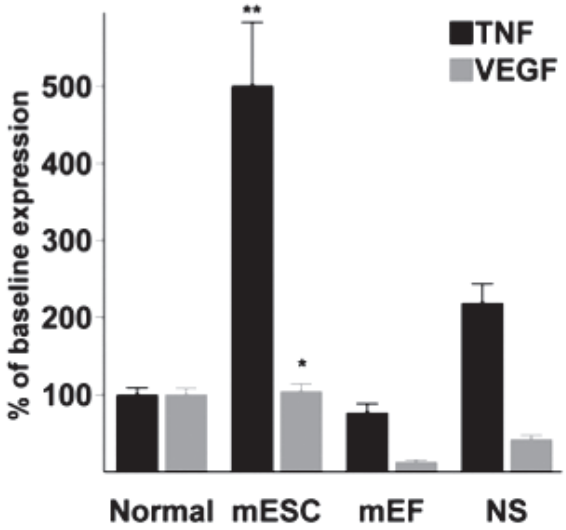

Figure 4. Relative quantitation of TNF-α and VEGF-A expression. Relative quantitation of mRNA expression on POD 7, normalized to the percentage of expression in normal, sham-operated hearts. A significant upregulation is noticeable in the mESC group. ** indicate p<0.01 vs. all groups, * indicates p<0.01 vs. mEF and NS (ANOVA).

Immunohistology of mESC cardiomyocyte differentiation. As seen in **figure 5** (**a-d**), cross-sectional images of H&E stained hearts demonstrate thinning of myocardial tissue and dilatation of LV chamber after LAD ligation. However, in the mESC treated mice, restoration of the LV wall mass and reduction of LV dilatation are seen. Co-localization of GFP with troponin and α-sarcomeric actin in isolated cells demonstrated potential differentiation of the mESC into cardiomyocytes as shown in **figure 5** (**e-h**). Colocalization of GFP with Connexin 43 suggest the formation of gap junctions as represented in **figure 5i**.

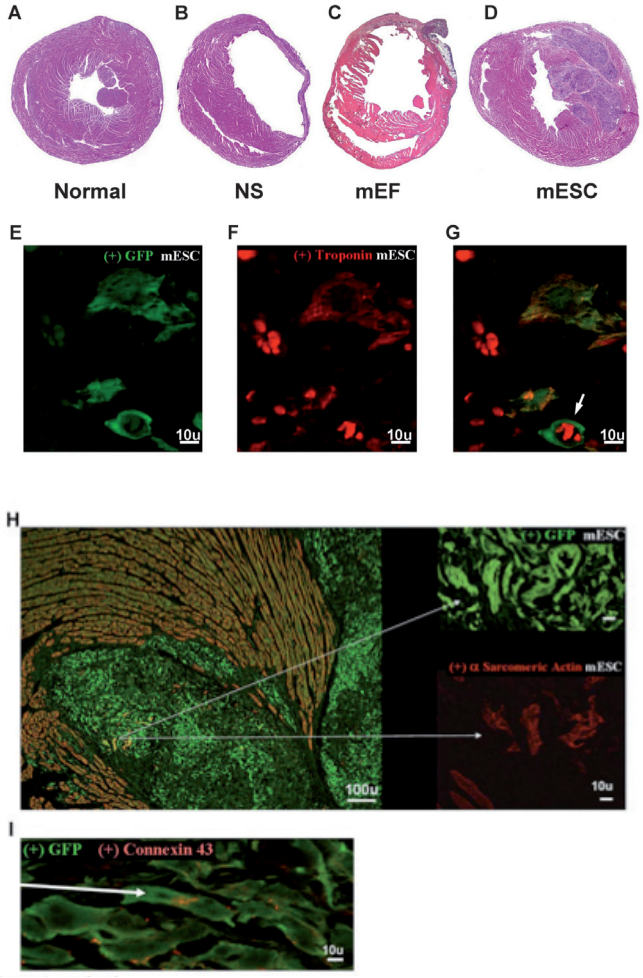

Figure 5. Histopathology of Anti-remodeling Effect and Cardiomyocyte Differentiation after mESC transplantation on POD 7. (a-d) Cross-sectional representative images of H&E stained (a) normal heart, (b) LAD ligation control, demonstrating thinning and dilatation of the ventricular wall, (c) mEF treated heart and (d) mESC treated heart demonstrating the restoration of the LV wall mass. (e) Confocal microscopy picture showing GFP positive stained mESC. (f) Confocal microscopy picture showing same cells as 5D expressing troponin. The 7-micron clustered round structures probably represent non-specifically stained red blood cells. (g) Overlay of 5D-E, showing co-localization of GFP with troponin, suggestive for a mESC-derived cardiomyocyte. Note that the non-specifically colored blood cells locate inside a GFP-stained blood vessel (white arrow), suggesting mESC- derived neovasculogenesis. (h) Image showing co-localization of GFP-positive mESC with alpha sarcomeric actin. (i) Image showing co-localization of GFP with connexin 43 (white arrow).

DISCUSSION

Cardiomyocyte death or dysfunction following an acute myocardial infarction (AMI) results in pathological remodeling of the left ventricle with eventual sequela of heart failure. Despite recent reports of the regenerative potential of cell-based therapies in the injured myocardium, a definitive mechanism of the enhanced myocardial function has not been elucidated. In the present study, we have provided independent support for *in vivo* MRI data by PV-loop and established the fundamental biological importance of cell survival, cell differentiation, and paracrine effects as potential mechanisms of mESC underlying myocardial restoration. The investigation focused on the immediate effects of cell transplantation post-AMI because teratoma formation would have likely interfered with reliable measurements during longer follow-up[15], as greatly increased mESC BLI signal on POD 14 confirmed. Our data demonstrated significantly improved LVEF measured by *in vivo* MRI, the most commonly utilized clinical end-point. This finding has been confirmed by end-systolic and maximal elastance values as measured by PV loop indicating improved systolic and diastolic functions as early as one week following mESC treatment. The improvement of diastolic function can be attributed to the augmentation of the infarct region's elasticity and recovery in the overall maximal elastance in the mESC-treated group. Moreover, we found a correlation between left ventricular volumes as measured by MRI and PV-loop.

These findings challenge the current notion that myocardial function is improved irrespective of cell type.[16, 17] The preservation of cardiac performance following cell transplantation cannot be attributed merely to the physical scaffolding effect but also must arise from the biological properties of the transplanted cells. During myocardial ischemia, the ischemic region develops diastolic and subsequent systolic abnormality.[18] Studies have confirmed the Frank-Starling relationship in which contractile function is preserved with reduction in ventricular volume.[19] In fact, our PV-loop results indicate a reduction in ventricular volume in the mESC group. This reduction involves complex yet fundamental biological processes. First, the prolonged survival kinetics of mESC can offer a longer lasting scaffolding effect, which may help to explain both the reduction in pathological remodeling and sustained restoration. More importantly, however, the persistence of viable mESC generates biologically active stimuli to salvage the injured myocytes. Thus, this enhanced survival of mESC enables a second potential mechanistic explanation for *in vivo* MRI findings of myocardial restoration: paracrine effect. The results from *ex vivo* TM-PCR demonstrate that the potential anti-apoptotic cytokine, TNF-a, was significantly upregulated in the mESC-treated group. TNF-α has been shown to have negative inotropic effects, to induce resistance to hypoxic stress in cardiomyocytes, and to play a role in the recruitment of stem cells.[20-23] It must be stated, however, that the increased TNF-a expression could also be attributable to a greater mass effect of mESC, with a subsequent greater endoge-

nous inflammatory reaction, a greater mESC-induced monocyte influx, or teratoma formation leading to endogenous TNF-a production. In addition, the observed up-regulation of VEGF-A in this study may promote angiogenesis to attenuate the ischemic insult to recover the injured cardiomyocytes. Finally, non-significant trends towards down-regulation of matrix metalloproteinase-1 (MMP-1) and procollagen 2α-1 have also been detected, which may contribute to decreased cardiac matrix remodeling in failing hearts.[24] Surprisingly, we did not observe upregulation of MMP-2 and -9. This may have been because the absence of T-cells in the SCID mice, on which MMP-2 and -9 expressions have been shown to depend.[25] Taken together, these TM-PCR results suggest that multiple mechanisms underlie the restoration by mESC.

The pluripotency of mESC may lead to regeneration of cardiac tissue after cardiomyogenic differentiation.26 In order to contract synchronously with host cardiomyocytes, newly formed mESC-derived cardiomyocytes must undergo electromechanical coupling through the formation of gap junctions *in vivo* with the host myocardium.26, 27 This study provides possible evidence that donor mESC are capable of engrafting within the host myocardium and differentiating into cardiomyocytes. While these findings are encouraging, it must be noted that this was a low-frequency event, making it less likely that the observed functional improvement can be attributed to robust cardiac regeneration by mESC-derived cardiomyocytes.

There are several limitations of this study. First of all, in order to investigate the acute effect of cell survival, we chose to compare fast-growing, undifferentiated mESC and less active mEF. This gave us the opportunity to study the relationship between cardiac function and cell survival in a relatively short period of one week. However, it must be stated that eventual teratoma formation, as suggested by our BLI findings on POD 14 and consistent with the literature[13, 15, 28], would likely hamper long term restoration of cardiac function. Secondly, this study does not provide insight in acute post-operative infarct size, which may have been dependent upon cell type. All operations, however, were conducted by the same experienced micro-surgeon that was blinded to the study. Moreover, after one week, all operated groups had a significant compromised LVEF on MRI, which lead to the assumption that infarct size had been comparable in all study groups. Third, we focused on validating the most important MRI data, namely LVED and LVES. Wall thickness, which could have correlated with cell survival, was not measured since we did not anticipate regenerative changes in the immediate period after AMI. Other studies are currently underway to address the regenerative changes by measuring wall thickness.

In conclusion, this is the first study to provide a fundamental functional and biological evaluation of *in vivo* MRI in mESC therapy. This study has shown that mESC are superior to mEF in restoring cardiac function in the immediate post-AMI period. A very fundamental notion that

the cells must at the very least survive to restore the myocardium is confirmed as the enhanced survival of mESC is attributed as one of the key factors in myocardial restoration. Improved survival of transplanted cells may not only offer a physical scaffolding mechanism but, more importantly, biological support by generating sustained paracrine effects after injury. We have also observed that mESC retain the ability to differentiate into cardiomyocytes, albeit at low frequency. Unfortunately, although the pluripotency and robust proliferation are among the major advantages of embryonic stem cells, these characteristics also contribute to teratoma formation[13, 15], which, for the present, prevents clinical translation. Further research regarding directed differentiation of mESC into cardiomyocytes may lead to a safe regenerative therapy for myocardial disease in the future.

ACKNOWLEDGEMENTS

We greatly appreciate the assistance in immunohistology from Ms. Pauline Chu and the help from Ms. Sally Zhang and Mr. Anant Patel with PCR. This work was supported by the NRSA Fellowship HL082447-01 (SLH), Donald W. Reynolds Foundation (PCY), Falk Cardiovascular Research Fund (RCR), NIH F32 and NIH K23 HL04338-01 (PCY).

REFERENCES:

1. Schachinger V, Erbs S, Elsasser A, Haberbosch W, Hambrecht R, Holschermann H, Yu J, Corti R, Mathey DG, Hamm CW, Suselbeck T, Assmus B, Tonn T, Dimmeler S, Zeiher AM. Intracoronary bone marrow-derived progenitor cells in acute myocardial infarction. *N Engl J Med.* 2006;355(12):1210-1221.
2. Chien KR. Stem cells: lost in translation. *Nature.* 2004;428(6983):607-608.
3. Kato S, Spinale FG, Tanaka R, Johnson W, Cooper Gt, Zile MR. Inhibition of collagen cross-linking: effects on fibrillar collagen and ventricular diastolic function. *Am J Physiol.* 1995;269(3 Pt 2):H863-868.
4. Kofidis T, de Bruin JL, Yamane T, Tanaka M, Lebl DR, Swijnenburg RJ, Weissman IL, Robbins RC. Stimulation of paracrine pathways with growth factors enhances embryonic stem cell engraftment and host-specific differentiation in the heart after ischemic myocardial injury. *Circulation.* 2005;111(19):2486-2493.
5. Li RK, Weisel RD, Mickle DA, Jia ZQ, Kim EJ, Sakai T, Tomita S, Schwartz L, Iwanochko M, Husain M, Cusimano RJ, Burns RJ, Yau TM. Autologous porcine heart cell transplantation improved heart function after a myocardial infarction. *J Thorac Cardiovasc Surg.* 2000;119(1):62-68.
6. Tomita S, Li RK, Weisel RD, Mickle DA, Kim EJ, Sakai T, Jia ZQ. Autologous transplantation of bone marrow cells improves damaged heart function. *Circulation.* 1999;100(19 Suppl):II247-256.
7. Arai T, Kofidis T, Bulte JW, de Bruin J, Venook RD, Berry GJ, McConnell MV, Quertermous T, Robbins RC, Yang PC. Dual *in vivo* magnetic resonance evaluation of magnetically labeled mouse embryonic stem cells and cardiac function at 1.5 t. *Magn Reson Med.* 2006;55(1):203-209.
8. Meyer GP, Wollert KC, Lotz J, Steffens J, Lippolt P, Fichtner S, Hecker H, Schaefer A, Arseniev L, Hertenstein B, Ganser A, Drexler H. Intracoronary bone marrow cell transfer after myocardial infarction: eighteen months' follow-up data from the randomized, controlled BOOST (BOne marrOw transfer to enhance ST-elevation infarct regeneration) trial. *Circulation.* 2006;113(10):1287-1294.
9. Orlic D, Kajstura J, Chimenti S, Jakoniuk I, Anderson SM, Li B, Pickel J, McKay R, Nadal-Ginard B, Bodine DM, Leri A, Anversa P. Bone marrow cells regenerate infarcted myocardium. *Nature.* 2001;410(6829):701-705.
10. Lunde K, Solheim S, Aakhus S, Arnesen H, Abdelnoor M, Egeland T, Endresen K, Ilebekk A, Mangschau A, Fjeld JG, Smith HJ, Taraldsrud E, Grogaard HK, Bjornerheim R, Brekke M, Muller C, Hopp E, Ragnarsson A, Brinchmann JE, Forfang K. Intracoronary injection of

mononuclear bone marrow cells in acute myocardial infarction. *N Engl J Med.* 2006;355(12):1199-1209.

11. Assmus B, Honold J, Schachinger V, Britten MB, Fischer-Rasokat U, Lehmann R, Teupe C, Pistorius K, Martin H, Abolmaali ND, Tonn T, Dimmeler S, Zeiher AM. Transcoronary transplantation of progenitor cells after myocardial infarction. *N Engl J Med.* 2006;355(12):1222-1232.
12. Kass DA, Midei M, Graves W, Brinker JA, Maughan WL. Use of a conductance (volume) catheter and transient inferior vena caval occlusion for rapid determination of pressure-volume relationships in man. *Cathet Cardiovasc Diagn.* 1988;15(3):192-202.
13. Swijnenburg RJ, Tanaka M, Vogel H, Baker J, Kofidis T, Gunawan F, Lebl DR, Caffarelli AD, de Bruin JL, Fedoseyeva EV, Robbins RC. Embryonic stem cell immunogenicity increases upon differentiation after transplantation into ischemic myocardium. *Circulation.* 2005;112(9 Suppl):I166-172.
14. Muller-Ehmsen J, Whittaker P, Kloner RA, Dow JS, Sakoda T, Long TI, Laird PW, Kedes L. Survival and development of neonatal rat cardiomyocytes transplanted into adult myocardium. *J Mol Cell Cardiol.* 2002;34(2):107-116.
15. Nussbaum J, Minami E, Laflamme MA, Virag JA, Ware CB, Masino A, Muskheli V, Pabon L, Reinecke H, Murry CE. Transplantation of undifferentiated murine embryonic stem cells in the heart: teratoma formation and immune response. *Faseb J.* 2007;21(7):1345-1357.
16. Jain M, DerSimonian H, Brenner DA, Ngoy S, Teller P, Edge AS, Zawadzka A, Wetzel K, Sawyer DB, Colucci WS, Apstein CS, Liao R. Cell therapy attenuates deleterious ventricular remodeling and improves cardiac performance after myocardial infarction. *Circulation.* 2001;103(14):1920-1927.
17. Weisel RD, Li RK, Mickle DA, Yau TM. Cell transplantation comes of age. *J Thorac Cardiovasc Surg.* 2001;121(5):835-836.
18. Bhatnagar SK, al-Yusuf AR. Left ventricular blood flow analysis in patients with and without a thrombus after first Q wave acute anterior myocardial infarction: two-dimensional Doppler echocardiographic study. *Angiology.* 1992;43(3 Pt 1):188-194.
19. Li RK, Mickle DA, Weisel RD, Zhang J, Mohabeer MK. *In vivo* survival and function of transplanted rat cardiomyocytes. *Circ Res.* 1996;78(2):283-288.
20. Chen Y, Ke Q, Yang Y, Rana JS, Tang J, Morgan JP, Xiao YF. Cardiomyocytes overexpressing TNF-alpha attract migration of embryonic stem cells via activation of p38 and c-Jun amino-terminal kinase. *Faseb J.* 2003;17(15):2231-2239.
21. Kurrelmeyer KM, Michael LH, Baumgarten G, Taffet GE, Peschon JJ, Sivasubramanian N, Entman ML, Mann DL. Endogenous tumor necrosis factor protects the adult cardiac myocyte against ischemic-induced apoptosis in a murine model of acute myocardial infarction. *Proc Natl Acad Sci U S A.* 2000;97(10):5456-5461.

22. Nakano M, Knowlton AA, Dibbs Z, Mann DL. Tumor necrosis factor-alpha confers resistance to hypoxic injury in the adult mammalian cardiac myocyte. *Circulation.* 1998;97(14):1392-1400.
23. Sivasubramanian N, Coker ML, Kurrelmeyer KM, MacLellan WR, DeMayo FJ, Spinale FG, Mann DL. Left ventricular remodeling in transgenic mice with cardiac restricted overexpression of tumor necrosis factor. *Circulation.* 2001;104(7):826-831.
24. Gunja-Smith Z, Morales AR, Romanelli R, Woessner JF, Jr. Remodeling of human myocardial collagen in idiopathic dilated cardiomyopathy. Role of metalloproteinases and pyridinoline cross-links. *Am J Pathol.* 1996;148(5):1639-1648.
25. Yu Q, Horak K, Larson DF. Role of T lymphocytes in hypertension-induced cardiac extracellular matrix remodeling. *Hypertension.* 2006;48(1):98-104.
26. Klug MG, Soonpaa MH, Koh GY, Field LJ. Genetically selected cardiomyocytes from differentiating embronic stem cells form stable intracardiac grafts. *J Clin Invest.* 1996;98(1):216-224.
27. Soonpaa MH, Koh GY, Klug MG, Field LJ. Formation of nascent intercalated disks between grafted fetal cardiomyocytes and host myocardium. *Science.* 1994;264(5155):98-101.
28. Cao F, Lin S, Xie X, Ray P, Patel M, Zhang X, Drukker M, Dylla SJ, Connolly AJ, Chen X, Weissman IL, Gambhir SS, Wu JC. *In vivo* visualization of embryonic stem cell survival, proliferation, and migration after cardiac delivery. *Circulation.* 2006;113(7):1005-1014.